Experimental study of linear and nonlinear regimes of density-driven instabilities induced by CO2 dissolution in water

R. Outeda, C. El Hasi, A. D'Onofrio, and A. Zalts
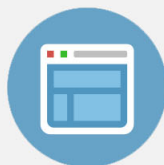
Experimental study of linear and nonlinear regimes of density-driven instabilities induced by CO$_2$ dissolution in water

R. Outeda,[1] C. El Hasi,[2] A. D'Onofrio,[1] and A. Zalts[2]

[1]*Grupo de Medios Porosos, Facultad de Ingeniería, Universidad de Buenos Aires, Paseo Colón 850, C1063ACV Buenos Aires, Argentina*
[2]*Instituto de Ciencias, Universidad Nacional General Sarmiento, J. M. Gutiérrez 1150, B1613GSX, Los Polvorines, Provincia de Buenos Aires, Argentina*

Density driven instabilities produced by CO$_2$ (gas) dissolution in water containing a color indicator were studied in a Hele Shaw cell. The images were analyzed and instability patterns were characterized by mixing zone temporal evolution, dispersion curves, and the growth rate for different CO$_2$ pressures and different color indicator concentrations. The results obtained from an exhaustive analysis of experimental data show that this system has a different behaviour in the linear regime of the instabilities (when the growth rate has a linear dependence with time), from the nonlinear regime at longer times. At short times using a color indicator to see the evolution of the pattern, the images show that the effects of both the color indicator and CO$_2$ pressure are of the same order of magnitude: The growth rates are similar and the wave numbers are in the same range (0–$30 \, \text{cm}^{-1}$) when the system is unstable. Although in the linear regime the dynamics is affected similarly by the presence of the indicator and CO$_2$ pressure, in the nonlinear regime, the influence of the latter is clearly more pronounced than the effects of the color indicator. © *2014 AIP Publishing LLC*.
[http://dx.doi.org/10.1063/1.4868040]

In this paper, we present density driven instabilities produced by CO$_2$ (gas) dissolution in water with a color indicator, in a Hele Shaw cell. The images were analyzed and instability patterns were characterized by mixing zone temporal evolution, dispersion curves, and the growth rate for different CO$_2$ pressures and different color indicator concentrations. Interesting results, that are not previously reported as far as we know, were obtained when comparing the behavior of this system in the linear regime of the instabilities (when the growth rate has a linear dependence with time), with the nonlinear regime at longer times. The main point of these results is that in the experiments done at short times using a color indicator to see the evolution of the pattern, the dynamics is affected by the presence of the indicator, but it has negligible effects at long times compared with the influence of CO$_2$ pressure.
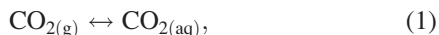
I. INTRODUCTION

The interest on instabilities in flows has focused on a broad scope of phenomena, such as assisted oil recovery, combustion, electrochemical depositions, reactive-diffusive systems, etc. For example, in assisted oil recovery, water is used to produce the movement of oil as water has a lower viscosity than oil, viscous fingering is produced affecting the dynamics of the system.[1] Spatial temperature differences[2]—characteristic of combustion processes—give rise to density differences, triggering instabilities. In electrochemical depositions or reactive-diffusive processes, the reaction kinetics and the diffusion coefficients must be taken into account to explain the observed instabilities at the reaction fronts.[3,4]

Also, fingering due to the effect of density and enthalpy changes on wave motion in reacting systems has been analyzed.[5,6]

In the same sense, in deep geologic CO$_2$ sequestration,[7–14] density driven instabilities can be expected: CO$_2$ is a soluble and reactive gas in water. Once it enters the aqueous phase, there is a density increase below the water surface because of the dissolution of the gas. Also, acid–base reactions take place with water (CO$_2$ is a weak acid, producing HCO$_3^-$ and CO$_3^=$), increasing the gas dissolution (at higher pH, a higher dissolution is produced). Chemical reactions in the aqueous phase can affect the instabilities triggered by density increases. Instabilities can be affected not only by different chemical and physical processes but also by heterogeneities in the system,[15,16] non-Newtonian character of the fluids,[17] magnetic fields,[18] etc.

Although CO$_2$ capture and deep geologic sequestration hold the promise to reduce emissions to the atmosphere associated with the use of carbon based fuels, and though there are some early pilot projects in different parts of the world, there is still an important lack of knowledge and more work is needed to put in full scale practice this important climate change mitigation technology and the associated regulatory framework.[19]

A deep understanding of buoyancy-driven phenomena due to CO$_2$ dissolution is important to account for geologic storage of this gas because they accelerate dissolution trapping, which favours long term sequestration. Mass transfer of CO$_2$ injected into a homogenous (sub)-surface porous formation saturated with a liquid was investigated by Farajzadeh *et al.*[20] They analyzed a porous medium, impermeable on the sides, that is exposed to CO$_2$ at the top. For

this configuration, density-driven natural convection enhances the mass transfer rate of CO_2 into the initially stagnant liquid. The presence of instabilities is inferred by the pressure difference between the measured values and those obtained through Fick's law. It is impossible to visualize instabilities in a 3D system like this, in contrast with a Hele Shaw cell (2D). On the other hand, many articles on experimental and/or theoretical aspects of geologic sequestration of CO_2, have been published lately.[21–27] For example, Kneafsey and Pruess[28,29] reported an experimental and theoretical analysis of CO_2 dissolution in a saline medium.

Buoyancy-driven hydrodynamic instabilities of acid–base fronts were studied both experimentally,[30] and theoretically[31,32] when an aqueous solution of a strong acid is placed above a denser aqueous solution of a color indicator in the gravity field. The neutralization reaction between the acid and the color indicator, as well as their differential diffusions, contributes to modify the initially stable density profile and trigger convective motions both above and below the initial contact line. A reaction-diffusion model based on charge balances and ion pair mobility was used to explain how the instability scenarios change when the concentrations of the reactants are varied.[32]

CO_2 dissolution in water increases its density: when CO_2 is injected into the Hele Shaw cell, it diffuses into the upper layer of the aqueous phase. This layer becomes denser, triggering instabilities. As CO_2 reacts with water, its solubility depends on chemical equilibrium between the different species

$$CO_{2(g)} \leftrightarrow CO_{2(aq)}, \tag{1}$$

$$CO_{2(aq)} + H_2O \leftrightarrow HCO_3^- + H^+, \tag{2}$$

$$HCO_3^- \leftrightarrow CO_3^= + H^+. \tag{3}$$

Different techniques can be used to get images of the buoyancy driven movements in a Hele Shaw cell. Interferometry and shadowgraphy, with different degrees of experimental and analytical complexity are based on refractive index variations due to concentration changes.[33] On the other hand, the main advantage of using color indicators is that it is the easiest way to obtain photographic images of the patterns to analyze, so it is a widespread technique. Of course, the fundamental hypothesis in this case is that the indicator has negligible effects on the hydrodynamics. When an

acid-base reaction takes place, properly chosen pH indicators can be used to detect pH changes in the system. In this case, there is an acid–base reaction of the dissolved CO_2 with the pH indicator (Bromocresol Green) modifying Eq. (2) in

$$CO_{2(ac)} + Ind^- + H_2O \leftrightarrow HInd + HCO_3^-, \tag{4}$$
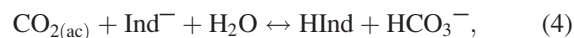
where Ind^- is the basic (blue) form of the color indicator and $HInd$ is its acid (yellow) form. This property was used to visualize instabilities involving acid base reactions.

Although acid-base reactions are typically exothermic, temperature plays virtually no role on the dynamics studied here in a Hele Shaw cell. Because of the high diffusivity of heat, the thermal density gradients can indeed be shown to be small compared with the solutal density gradients.[34]

Nevertheless, we recently observed[31,32] that the pH indicator can achieve an active role, affecting the hydrodynamics of the system. When fluids, such as HCl and NaOH solutions are put in contact in an initially stable density array, and the instability development was observed by interferometry,[34] a different pattern was obtained than that observed with the pH indicator. These results were confirmed experimentally and numerically:[31] the differences are due to differential diffusion processes.[32]

In this work, we examine the buoyancy driven instabilities observed in an aqueous solution containing a color indicator under a CO_2 atmosphere in the linear and nonlinear regimes. The instability patterns were studied varying the pressure of CO_2 and the concentration of the indicator.

II. EXPERIMENTAL

The experimental setup is shown in Figure 1. It consists of a vertically oriented Hele Shaw cell specially designed to work with gases at different pressures. The cell was built with two 12 mm thick acrylic plates and a diameter of 10 cm, with 1 mm gap obtained with a spacer. An o-ring was used to seal the compartment so it became gas tight, and the plates were held together with 12 equidistant screws. There are four inlets, with different valves to allow the injection of rinsing and working solutions (valve 4), as well as purging with N_2 or filling with CO_2 at a desired pressure (valve 1). Valves 2 and 3 are used as exhaust. There is an auxiliary valve (5) used to fill or rinse the cell. To observe the effects of CO_2 dissolution, during each experiment, a constant CO_2
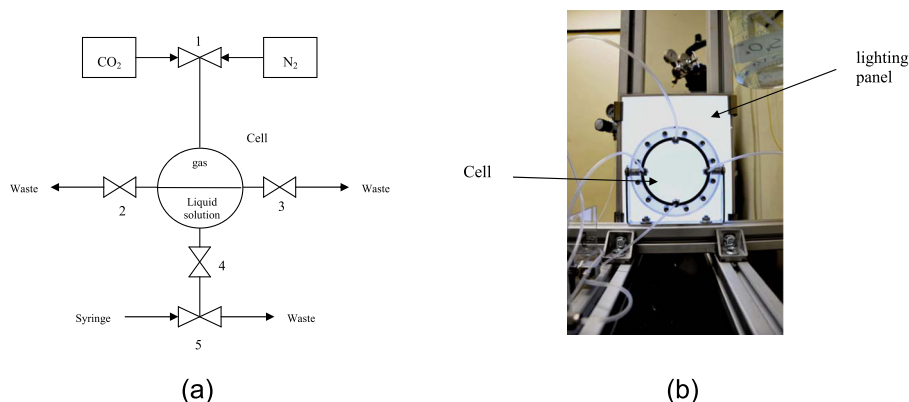

FIG. 1. Experimental set-up. (a) Scheme: to load CO_2 or N_2, valve 1 is used; valves 2, 3 level the liquid, the solutions are injected into the cell using valve 4, and valve 5 is an auxiliary device used for rinsing or loading the cell. (b) Photo of the device and lighting panel.

pressure was held in contact with the aqueous solution filling about half of the cell. To avoid a premature reaction of CO_2 with the solution during the injection of the aqueous phase, the cell was previously purged and loaded with N_2 and the solution was injected with a syringe through valves 4 and 5. Once the solution was in place at exit level (valves 2 and 3), N_2 was replaced by CO_2 to start the experiment. Bromocresol Green was used as color indicator[32] to visualize the CO_2 dissolution pattern. All experiments were carried out at room temperature (25 °C).

The Hele Shaw cell was illuminated with transmitted diffuse white light from behind, and the experiments were recorded with a digital camera (3072 × 2304 pixels). Images, obtained every 3 s, were stored and analysed splitting in RGB channels, choosing the channel with the highest black-white contrast. This procedure was employed to determine the position of the reaction front, the growth rate as a function of wave number, the pattern wavelength, and the length of the mixing zone as a function of time. This procedure was carried out with programs based on language C, developed in the laboratory.

III. RESULTS

When CO_2 is present in the headspace of the Hele Shaw cell containing a solution of the colour indicator in its basic form (green-blue), the gas dissolves increasing the solution density. CO_2 (aq) is an acid and therefore it reacts with the Bromocresol Green, changing its color to yellow. A thin yellow line appeared almost instantaneously behind the interface once the CO_2 tank was connected to the cell (displacing the N_2 that was used to purge the cell), indicating the onset of the reaction (t = 0 corresponds to the moment that N_2 was displaced and the system takes the work pressure). The position of the front is defined by the line of separation between the yellow and blue region. The instabilities appear a few seconds later (10 s approximately). CO_2 mass influx at the boundary layer produced the local density increase at the reaction front needed to trigger the instabilities; an example of the sequential finger like pattern development over time is shown in Figure 2. The yellow fingers invade the liquid downwards and it is clearly seen that as the process goes on, fingering takes place maintaining the wave number at the tip of fingers (k_b), whereas at the interface, the wave number (k_i) decreases. The wave numbers are determined counting the number of fingers at the bottom and the top, using the length scale shown in the figure. For Figure 2, k_b at t = 60 s, 90 s, and 120 s is, in all cases, (21 ± 1) cm^{-1}, whereas k_i is (21 ± 1) cm^{-1} at t = 60 s, but at t = 90 s and 120 s, k_i decreases to (20 ± 1) cm^{-1} and (15 ± 1) cm^{-1}, respectively. This finger merging at the interface is opposite to the viscous fingering pattern, which is characterized by tip splitting. This is one of the most important differences found with respect to other reactive and hydrodynamically unstable systems.

Experiments were done under different conditions: (a) varying the concentration of the pH indicator in the aqueous phase from 3.2×10^{-5} M to 6.4×10^{-4} M, at a fixed CO_2 pressure (3.0 atm); (b) varying the CO_2 pressure between 1.5 and 5.0 atm, at a fixed pH indicator concentration
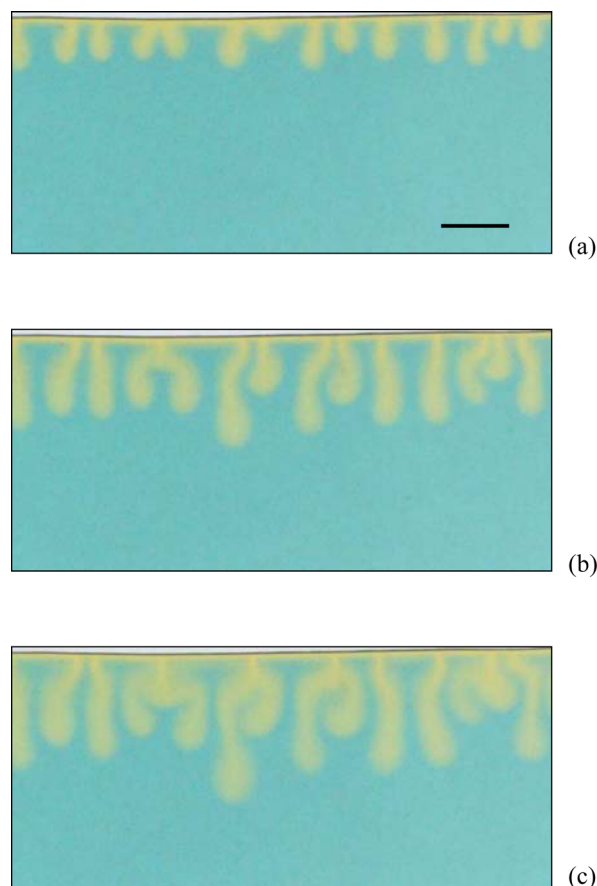

FIG. 2. Example of convective instability for CO_2 (g) (3.0 atm) and Bromocresol green (3.2×10^{-4} M), shown at (a) 60 s, (b) 90 s, and (c) 120 s. The upper dark horizontal area is a shadow of the interface between the gas and liquid phases. The black bar is 0.5 cm long.

(3.2×10^{-4} M). Series of four replicates were done for each condition, and average values were reported.

A. Variable concentration of the color indicator

The concentration of the color indicator was modified between 3.2×10^{-5} M and 6.4×10^{-4} M, at a constant CO_2 pressure (3.0 atm). In all cases, a narrow yellow layer was visible at the interface about 6 s after starting the experiment. Although CO_2 was present in this yellow area of the aqueous phase, no instabilities were detected. Figure 3 shows that after 99 s, instabilities are clearly seen in all cases. Furthermore, there are no significant differences in the mixing zone (nonlinear regime), defined as the region parallel to the interface where the concentration of the acidic solution lies between 5% and 95%. A set of four experiments were done for each concentration. The wave number (k_b) was also of the same order of magnitude for the variation of concentration of the indicator: $(14 \pm 1$ and $19 \pm 1)$ cm^{-1}, for the set shown in Figure 3.

Figure 4 shows the temporal evolution of the mixing length for the four studied concentrations of the indicator. After approximately the first 30 s, where the mixing length is constant, a sharp increase indicates the evolution of a convective process, similar for the four cases. At t = 100 s, the difference between the highest and lowest mixing length is
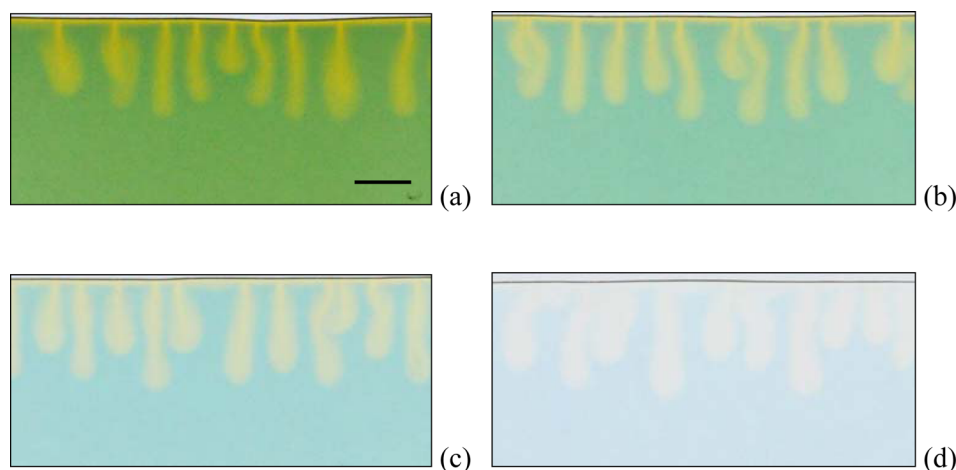
FIG. 3. Convective patterns observed at $t = 99$ s for various values of the concentrations of the color indicator: (a) 6.4×10^{-4} M, (b) 3.2×10^{-4} M, (c) 1.6×10^{-4} M, and (d) 3.2×10^{-5} M. The CO_2 pressure is equal to 3.0 atm. The black bar is 0.5 cm long.

about 16%, but, as a cross between the mixing lengths of the extreme concentrations is seen, it is impossible to establish a more definite trend.

Figure 5(a) shows three examples of the dispersion curves, representing the growth rate corresponding to the different wave numbers at the unstable front. The growth rate was obtained applying the Fourier transform to the wave fronts (1D signal corresponding to the separation line between the yellow and blue region). As this analysis was done during the linear regime of the instabilities (when the growth rate has a linear dependence with time), the analyzed wave number was k_b. For each concentration, a set of four experiments were done, and average values, as well as the maximum and minimum are given in Figure 5(a); these results were fitted with a quadratic function just to guide the eye.

The wave numbers (k_{max}) corresponding to the highest growth rate (σ_{max}) resulted similar for the different concentrations. Nevertheless, growth rate increased when the concentrations were higher. This trend can be observed in Figure 4 (for times shorter than 30 s) and more clearly, in Figure 5(b).

B. Variable CO_2 pressure

Figure 6 shows a higher development of the instability patterns obtained when CO_2 pressure was varied between 1.5

and 5.0 atmospheres, with a constant indicator concentration (3.2×10^{-4} M). Clearly, larger mixing lengths were obtained increasing the CO_2 pressure (Figure 7). A higher CO_2 pressure at the boundary layer increased the mass influx to the aqueous phase, increasing as well the density of the solution at the interface.

Figure 7 shows that the instabilities were triggered at different times depending on CO_2 pressure. For the lowest CO_2 pressure (1.5 atm), the instabilities were seen at about

(a)

(b)

FIG. 5. (a) Dispersion curve for different values of concentration of the pH indicator. (b) Growth rate σ_{max} as a function of pH indicator. A set of four experiments were done for each concentration, and the average values, as well as the maximum and minimum are given.
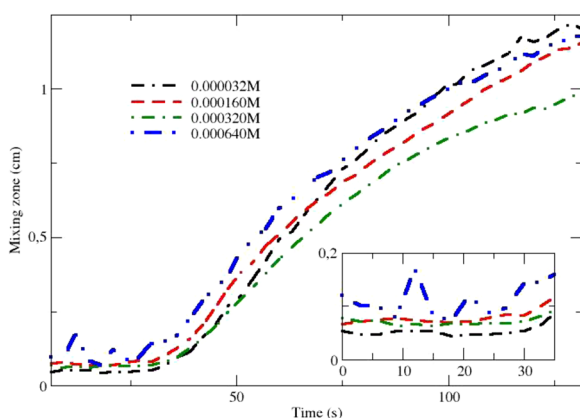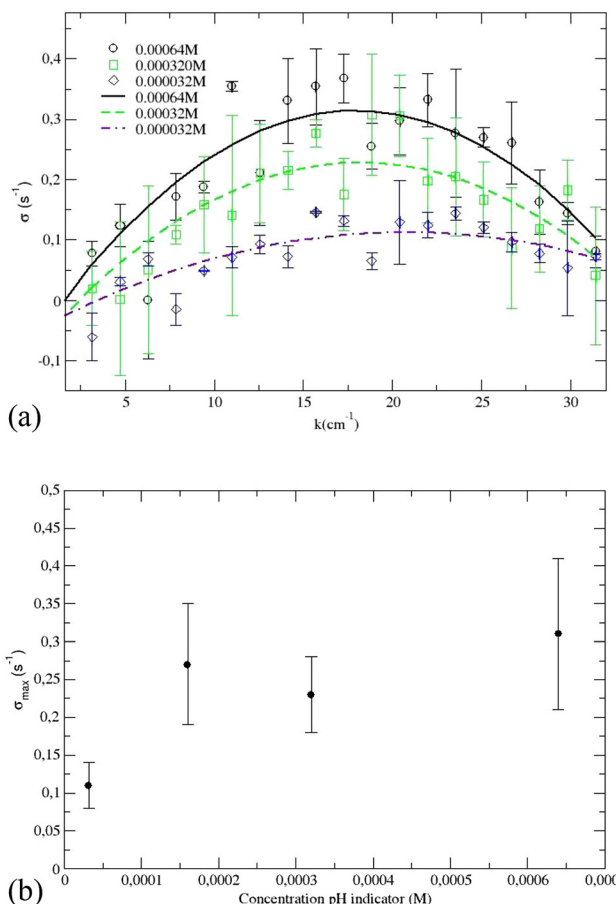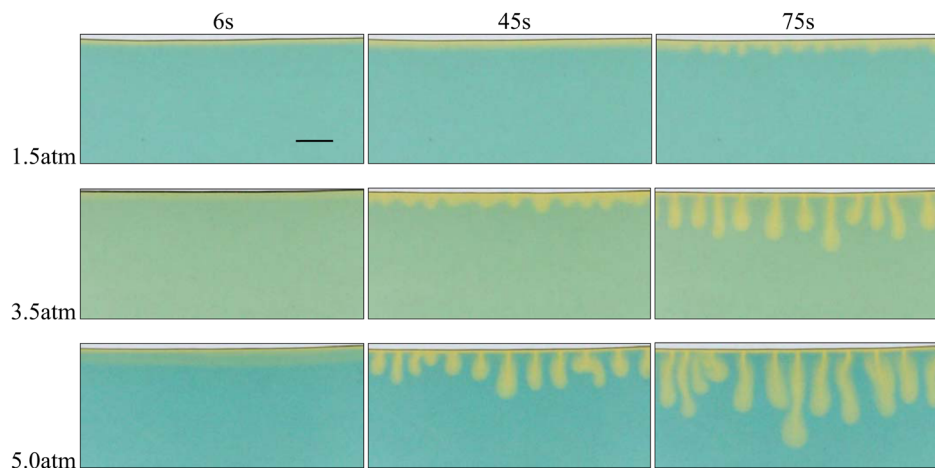

FIG. 4. Mixing zone as a function of time for four different concentrations of the color indicator, corresponding to the experimental conditions of Fig. 3. Error of measurement 0.004 cm.

FIG. 6. Convective patterns observed at $t = 6$ s, 45 s, and 75 s for different CO_2 pressures. Concentration of the color indicator is 3.2×10^{-4} M. The black bar is 0.5 cm long.

60 s after starting the experiment. A decreasing trend was observed as the pressure was increased, reaching to 10 s when the pressure was 5.0 atm. This behavior is clearly in contrast with that observed varying the concentration of the color indicator (Figure 4), where for all the concentrations the instability triggering time was about 30 s. On the other hand, Figure 8 shows the mixing lengths for $t = 100$ s at different CO_2 pressures. In this case, a difference of 83% between the experiments at higher and lower pressures was obtained.

Dispersion curves were obtained for the system varying CO_2 pressures, using the previously described methodology. Three examples are shown in Figure 9, leading to similar observations to those previously given varying the concentration of the indicator: although k_{max} has not a clear behavior for different pressures, the growth rate increased with the pressure. This trend is shown in Figures 7 (for times shorter than 20 s) and 9(b) (σ_{max} vs CO_2 pressure).

IV. DISCUSSION

In this article, we have studied an acid base reaction taking place in an initially stable density field (CO_2 (g)–aqueous phase). The system is different from those previously reported by our group[30–32] because the reactive species were confined to the lowest part of the cell (liquid phase), so a differential diffusive process is not adequate to explain the observed patterns. CO_2—being highly soluble in water—dissolves readily in the aqueous phase producing a local density increase. This CO_2 mass influx at the boundary layer can trigger Rayleigh-Taylor type instabilities.

The buoyancy effect produced by the instabilities gave rise to convective movements at the interface, decreasing the initial wave number (k_b). Nevertheless, this wave number k_b was conserved deeper in the aqueous solution during the propagation of the fingering. The merging of the fingers (or the decrease in the wave number at the interface between the gaseous CO_2 and the aqueous solution) was different from that observed when hydrodynamic instabilities are triggered by viscosity, where the merging takes place at the tips of the fingers. In this case, there was no tip splitting: the wavenumber of the tips remained the same through the evolution of the instabilities.

The experimental results showed that the instabilities observed as a consequence of the dissolution of CO_2 in water and further reaction with the pH indicator was independent from the concentration of the indicator, at least when the system was under a nonlinear regime (for longer times). The induction time, the mixing lengths, the wave number, and the shape of the fingers were similar for all the
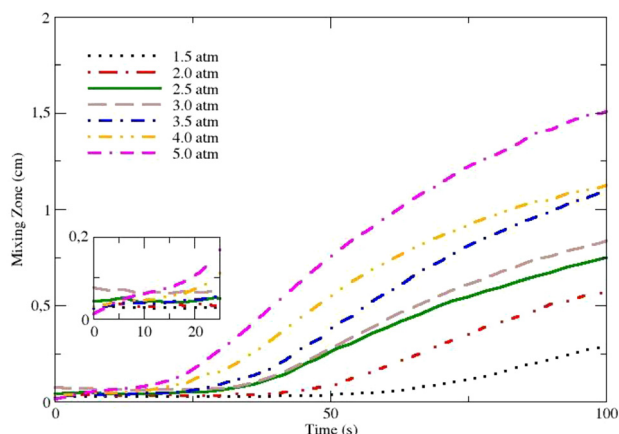

FIG. 7. Temporal evolution of the mixing zone for different CO_2 pressures. Error of measurement 0.004 cm.
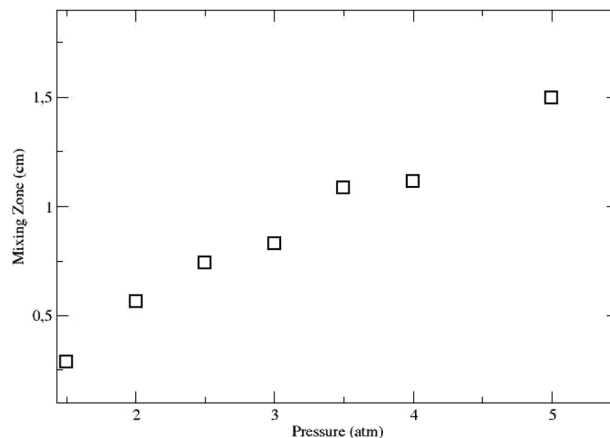

FIG. 8. Mixing zone as a function of pressure for time equal to 100s. Error of measurement 0.004 cm.
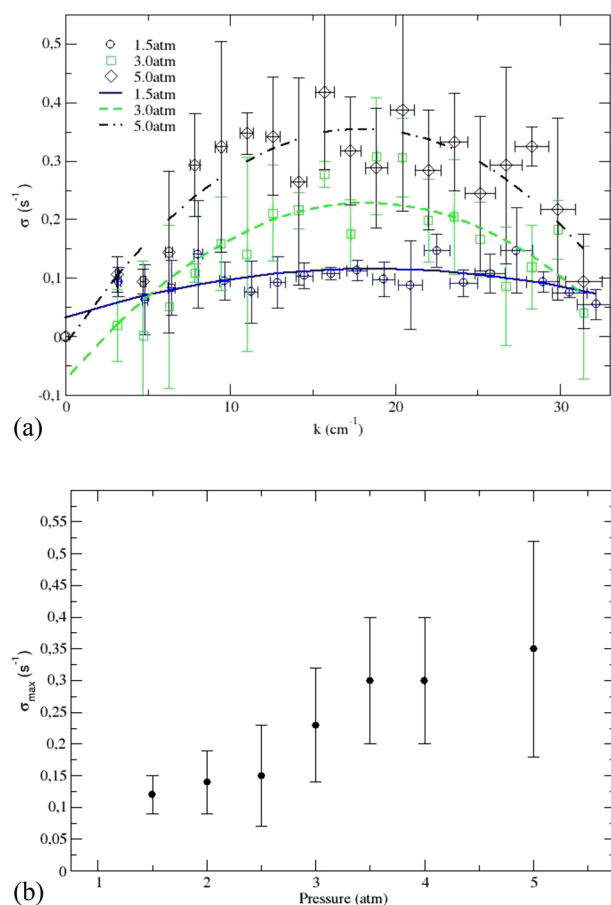
(a)

(b)

FIG. 9. (a) Dispersion curves for different CO_2 pressures. (b) Growth rate (σ_{max}) for different CO_2 pressures. A set of four experiments were done for each pressure, and the average values, as well as the maximum and minimum are given.

(a)

(b)

FIG. 10. (a) Wave number as a function of CO_2 pressure; the average value of k_{max} is equal to 18.65 cm^{-1}. (b) Wave number as a function of concentration of color indicator; the average value of k_{max} is equal to 19.29 cm^{-1}.

concentrations of the pH indicator used in the experiments. When CO_2 pressure was modified, the wave number and the shape of the fingers were independent from the pressure, but induction times decreased and mixing lengths increased when the pressure was increased.

A more detailed analysis of the mixing lengths for long times (t = 100 s) showed that variability is more pronounced when the pressure was modified (83%, 1.5–5.0 atm) than in the case of varying the concentration of the color indicator (16%, 3.2×10^{-5} M–6.4×10^{-4} M). These results suggest that in this system, the role of the color indicator is negligible in the development of the instabilities. When a linear stability analysis was performed, both the color indicator and the CO_2 pressure showed a similar influence on the fingering. This is suggested by the dispersion curves: they are similar for both types of experiments. Varying the concentration of the color indicator or CO_2 pressures, Figure 10 shows that there is no clear trend in the wave number with the highest growth rate k_{max}. Growth rates were between 0.15 s^{-1} to 0.36 s^{-1} varying concentrations and pressures. The values of k_{max} and their growth rate were obtained fitting the data with a quadratic function in the dispersion curves. Although these fittings were done just to guide the eye and they did not have any physical meaning, they help to identify trends varying some parameters of the system (concentration and pressure,
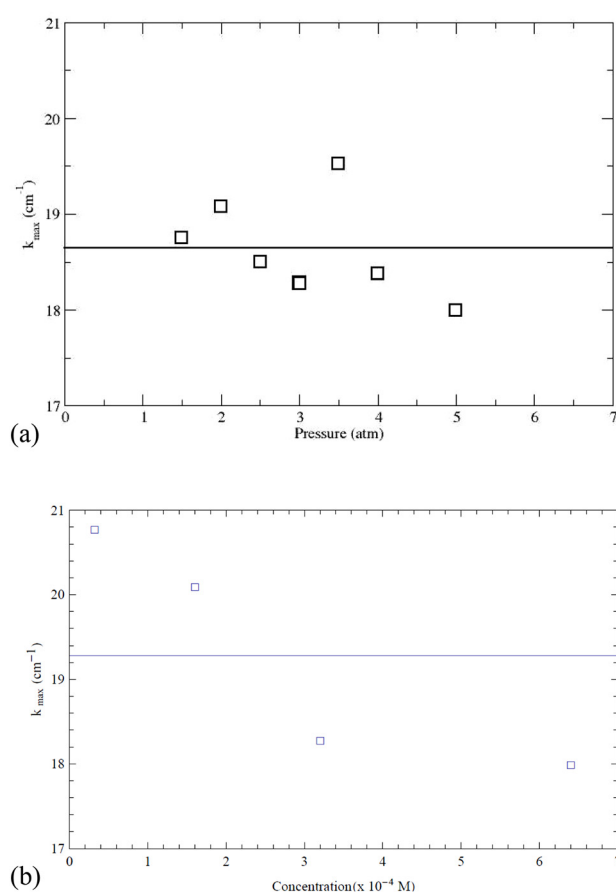
in this case). In all cases, the growth rate was calculated during the first 30 s, a time interval where the system behaved linearly. As it was stated earlier, there was no clear trend with the concentration or the pressure, in accordance with Figures 3 and 6, where the wave number was similar for all the cases (average value of k_{max} is equal to 18.65 cm^{-1} and 19.29 cm^{-1} for CO_2 pressure and color concentration, respectively). Also, the wave numbers from which the growth rates became negative were similar for all the pressures and concentrations (see Figures 5 and 9). This suggests that the shape of the waves generated at the interface was similar although variability was observed for the growth rate of the instabilities (see Figures 3 and 6).

V. CONCLUSIONS

The use of a color indicator to detect the instabilities generated by the dissolution of CO_2 in a liquid phase can affect the dynamics of the system during its linear development stage (at short times). The influence of modifying concentrations of the indicator was of the same order of magnitude as varying the CO_2 pressure. On the other hand, once the system reached the nonlinear development stage (at long times), varying the concentration of the pH indicator had negligible effects compared with those of the pressure.

Increasing CO_2 pressure increased the amplitude of the instabilities, but had no effects on the wave number and the

shape. We expected an increase in the wavenumber with increasing pressure, but the experimental data show that the system has an unusual behavior. This observation calls for further theoretical studies. On the other hand, higher pressures produced greater CO_2 mass influx at the boundary layer leading to a faster fingering growth.

ACKNOWLEDGMENTS

[1] G. M. Homsy, Annu. Rev. Fluid Mech. **19**, 271 (1987).

[2] G. García Casado, L. Tofaletti, D. Müller, and A. D'Onofrio, J. Chem. Phys. **126**, 114502 (2007).

[3] J. Yang, A. D'Onofrio, S. Kalliadasis, and A. De Wit, J. Chem. Phys. **117**, 9395 (2002).

[4] D. Lima, A. D'Onofrio, and A. De Wit, J. Chem. Phys. **124**, 014509 (2006).

[5] J. A. Pojman, I. R. Epstein, T. J. McManus, and K. Showalter, J. Phys. Chem. **95**, 1299 (1991).

[6] J. A. Pojman, A. Komlósi, and I. P. Nagy, J. Phys. Chem. **100**, 16209 (1996) and the references there in.

[7] M. L. Szulczewski, L. Cueto-Felgueroso, and R. Juanes, Energy Proc. **1**, 3421 (2009).

[8] R. T. Okwen, M. T. Stewart, and J. Cunningham, Int. J. Greenhouse Gas Control **4**, 102 (2010).

[9] P. Stauffer, H. Viswanathan, R. Pawar, and G. Guthrie, Environ. Sci. Technol. **43**, 565 (2009).

[10] G. Ravagnani, E. L. Ligero, and S. B. Suslick, J. Pet. Sci. Eng. **65**, 129 (2009).

[11] L. Zhao, L. Sang, J. Chen, J. Ji, and H. Teng, Environ. Sci. Technol. **44**, 406 (2010).

[12] P. C. Lin, C. W. Huang, C. Hsiao, and H. Teng, Environ. Sci. Technol. **42**, 2748 (2008).

[13] G. Montes-Hernandez, R. Pérez-López, F. Renard, J. M. Nieto, and L. Charlet, J. Hazard. Mater. **161**, 1347 (2009).

[14] S. J. Gerdemann, W. O'Connor, D. Dahlin, L. Penner, and H. Rush, Environ. Sci. Technol. **41**, 2587 (2007).

[15] L. Macias, D. Müller, and A. D'Onofrio, Phys. Rev. Lett. **102**, 094501 (2009).

[16] C. T. Tan and G. M. Homsy, Phys. Fluids A **4**, 1099 (1992).

[17] A. Lindner, P. Coussot, and D. Bonn, Phys. Rev. Lett. **85**, 314 (2000).

[18] C. Flament, G. Pacitto, J. C. Bacri, I. Drikis, and A. Cebe, Phys. Fluids **10**, 2464 (1998).

[19] E. Wilson, M. Morgan, J. Apt, M. Bonner, C. Bunting, J. Gode, R. Hazseldine, C. Jaegger, D. Keith, and S. McCoy, Environ. Sci. Technol. **42**, 2718 (2008).

[20] R. Farajzadeh, H. Salimi, L. J. Pacelli, P. L. J. Zitha, and H. Bruining, Int. J. Heat Mass Transfer **50**, 5054 (2007).

[21] R. Farajzadeh, A. Barati, H. A. Delil, J. Bruining, and P. L. J. Zitha, Pet. Sci. Technol. **25**, 1493 (2007).

[22] C. J. Seto and G. J. M. Crae, Environ. Sci. Technol. **45**, 845 (2011).

[23] B. Liu and Y. Zhang, Environ. Sci. Technol. **45**, 3504 (2011).

[24] P. Gruene, A. G. Belova, T. M. Yegulalp, R. J. Farrauto, and M. J. Castaldi, Ind. Eng. Chem. Res. **50**, 4042 (2011).

[25] Y. Zhang, F. Chan, Y. Son, J. Zhao, Y. Zhan, and W. Jian, J. Chem. Eng. Data **56**, 565 (2011).

[26] X. Han, Z. Yu, J. Qu, T. Qi, W. Guo, and G. Zhang, J. Chem. Eng. Data **56**, 1213 (2011).

[27] B. Han, C. Zhou, J. Wu, D. J. Tempel, and H. Cheng, J. Phys. Chem. Lett. **2**, 522 (2011).

[28] T. J. Kneafsey and K. Pruess, Energy Proc. **4**, 5114 (2011).

[29] T. J. Kneafsey and K. Pruess, Transp. Porous Media **82**, 123 (2010).

[30] A. Zalts, C. El Hasi, D. Rubio, A. Ureña, and A. D'Onofrio, Phys. Rev. E **77**, 015304(R) (2008).

[31] C. Almarcha, P. M. J. Trevelyan, L. Riolfo, A. Zalts, C. El Hasi, A. D'Onofrio, and A. De Wit, J. Phys. Chem. Lett. **1**, 752 (2010).

[32] S. Kuster, L. A. Riolfo, A. Zalts, C. El Hasi, C. Almarcha, P. M. J. Trevelyan, A. De Wit, and A. D'Onofrio, Phys. Chem. Chem. Phys. **13**(38), 17295 (2011).

[33] C. Wylock, S. Dehaeck, A. Rednikov, and P. Colinet, Microgravity Sci. Technol. **20**, 171 (2008).

[34] C. Almarcha, P. M. J. Trevelyan, P. Grosfils, and A. De Wit, Phys. Rev. Lett. **104**, 044501 (2010).